



OPEN

Experimental and Monte Carlo-based health risk assessment of seasonal radon exposure in groundwater and soil of Meghalaya, India

Hari Prasad Jaishi¹  , Devashree Borgohain¹, Ramesh Chandra Tiwari²,
Shanborlin Khardewsaw¹, Saidur Rahman¹ & Arif Zaman¹

This study examines seasonal changes in radon levels in groundwater and soil, and their related health risks, in Baridua Village, Meghalaya, India. Groundwater and soil samples were collected during summer (Aug-Sep 2024) and winter (Jan-Feb 2025). Radon in water was measured using emanometry technique, while soil radon, radium content, and exhalation rates were determined with LR-115 detectors. Groundwater radon was significantly higher in summer (57.87 Bq L^{-1}) than in winter (29.30 Bq L^{-1}), with 93% of summer samples exceeding the USEPA safe limit of 11.1 Bq L^{-1} . The mean soil radon concentrations were 938.57 Bq m^{-3} in summer and 777.14 Bq m^{-3} in winter, suggesting relatively small variations. Soil radium content and exhalation rates were observed to be below the global average values. During summer, total effective doses due to radon in water exceeded the WHO guideline of $100 \mu\text{Sv y}^{-1}$, with average values of $137.72 \mu\text{Sv y}^{-1}$ for adults and $147.46 \mu\text{Sv y}^{-1}$ for children. Monte Carlo simulations indicated a 48.91% chance that children may exceed this dose. Soil radon contributed little to alpha radiation dose, with only a 0.73% probability of exceeding the limit under worst-case conditions.

Keywords Radon, Groundwater, Soil, Seasonal variation, Health risk, Monte carlo simulation

Radon (Rn-222) is natural radioactive gas formed by the decay of uranium (U-238) in soil and rocks. It can pose significant health risks when present in elevated levels. Radon can migrate through soil pores and enter groundwater, particularly in areas with high uranium content^{1,2}. Once dissolved in water, radon can release into the air during household water use, contributing to indoor radon exposure and can also be ingested directly, leading to internal exposure. These exposures are linked to increased risks of lung and stomach cancer, as recognized by organizations such as the WHO and UNSCEAR, which classify radon as a Group 1 carcinogen^{3,4}. Monitoring radon in soil and water is therefore essential for assessing its distribution, identifying pathways into human environment, and evaluating associated health risks. Estimating annual effective doses for both inhalation and ingestion helps understand cumulative impacts, as dose levels vary with radon concentration, exposure duration and population vulnerability (e.g., children vs. adults).

The study area in Meghalaya features hilly terrain with steep slopes and intermontane valleys, primarily composed of Archaean Gneissic Complex rocks, intrusive granites, quartzites, and phyllites of the Precambrian Shillong Group. The gneissic rocks are often fractured and fissured, and soils range from loamy to clay, typically dark reddish-brown, slightly to moderately acidic, and rich in organic carbon with medium phosphorus and potassium content and high micronutrient levels⁵. Meghalaya holds significant uranium potential, particularly in the Mahadek Basin, where sandstone-type uranium mineralization occurs. Uranium reserves are estimated at about 9,500 tons, with major deposits in Domiasiat and Wahkyn, hosted mainly in sandstones of the Cretaceous Mahadek Formation underlain by the Precambrian Gneissic Complex and Shillong Group rocks^{6,7}. In Ri-Bhoi district, mining activities targeting minerals such as granite and limestone can disturb the underlying rocks, increasing background radiation and facilitating radon release into the atmosphere.

¹Department of Physics, University of Science and Technology Meghalaya, Baridua 9th Mile, Meghalaya 793 101, India. ²Department of Physics, Mizoram University, Aizawl 796 004, India.  email: harijaishi.ustm@gmail.com

Although indoor radon measurements have been carried out in different locations of Meghalaya^{8–12}, very few studies have reported soil radium content and radon exhalation rates^{13,14}, and none have documented groundwater radon levels in the Ri-Bhoi district which leave a significant gap in understanding radon exposure in this region. Since soil and the underlying rocks are the main sources of radon in both indoor air and ground water, assessing soil radon, exhalation rates and groundwater radon concentrations is crucial for evaluating potential exposure. In the study area, the groundwater is drawn directly from wells. Residents either used immediately or pump it into overhead tanks for household distribution. In both cases, water is used without any treatment or significant delay, and no materials such as filtration systems or long duration holding tanks are used that could alter the radon concentration significantly. While sampling from household taps could better reflect exposure due to possible radon loss during storage, this effect is minimal here, as water is typically used within three to four hours and pumped multiple times a day. Sampling directly from wells thus provide a valid representation of actual exposure.

The present investigation, conducted during August–September 2024 and January–February 2025 in Baridua village, Ri-Bhoi district, Meghalaya, measured soil radon concentration, radium content, surface and mass exhalation rates, and groundwater radon levels, and estimated the radiation doses received by individuals via inhalation and ingestion. The August–September period in Ri-Bhoi is sometimes referred to as “summer” due to the late monsoon warmer conditions. The district climate varies from pleasant summers and cold winters in the highlands to hot, humid summers and cool winters in the lowlands bordering the Brahmaputra plains¹⁵. The location map and sampling points are shown in Fig. 1, where both soil and water were collected at each site. Health risk assessment was performed using two approaches: (i) fixed-parameter calculations based on experimentally measured concentrations and standard conversion factors, and (ii) stochastic simulation using the Monte Carlo Simulation (MCS) technique, which generates random samples from an assumed log-normal dose distribution to represent variability. Simulations were carried out in Python 3. Previous studies have successfully applied MCS to radon health risk assessment, demonstrating its effectiveness in characterizing dose distributions and estimating risk probabilities^{16–18}.

Materials and methods

Groundwater and soil samples were collected from a residential area during the summer (August–September 2024) and winter (January–February 2025) seasons. A total of 30 samples were collected, comprising 15 groundwater and 15 soil samples in each season. The soil sampling locations were selected using the Simple Random Sampling method as recommended by the IAEA guidelines¹⁹. This involved arbitrary selection of sampling points within the defined study area, with coordinates determined from random number tables to ensure independent and unbiased coverage. To adequately represent spatial variation, sampling points were placed at approximately regular intervals, providing broad coverage of the study area while maintaining the randomness required by the method. For spatial comparison, groundwater samples were taken from wells located in close proximity to the respective soil sites, enabling consistent and reliable correlation between soil and groundwater radon concentrations. Details of sample collection and analysis are described in the subsequent section.

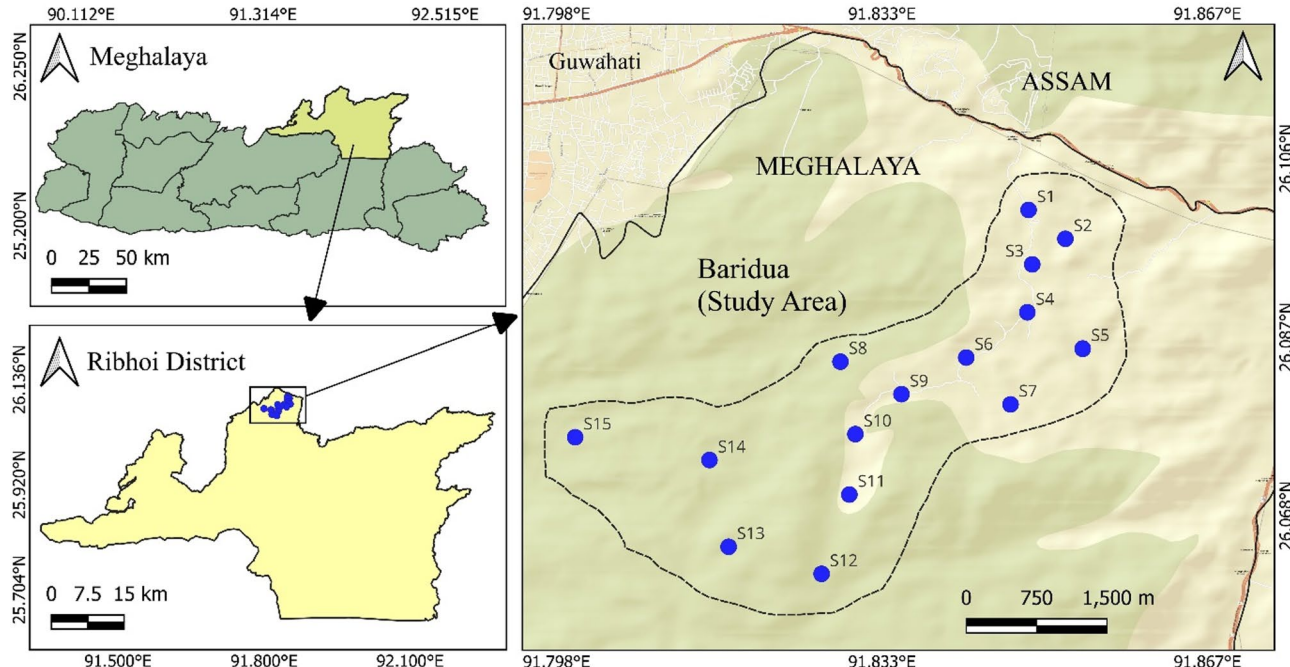


Fig. 1. Location map of the study area with sample collection points.

Radon measurements in water samples

Groundwater samples were collected using airtight 250 mL polypropylene bottles to preserve sample integrity. Three samples were taken from each location, and the final radon concentration (^{222}Rn) was calculated as the average. Care was taken during collection to avoid bubble formation and prevent radon loss. Samples were analysed following American Society for Testing and Materials protocols²⁰ and were immediately transported to the laboratory after collection. Radon concentrations were determined by the emanometry technique, which detects radon released from agitated water samples²¹.

The setup (Fig. 2) included a radon bubbler, a Lucas cell, and a programmable counting system. The bubbler, made from Corning glass, features a leak-proof sintered disc, airtight joints, PTFE stopcocks, and secure couplings for gassing, degassing, and radon transfer. The Lucas cell is a 150 cm³ cylindrical chamber internally coated with ZnS (Ag) scintillator powder, equipped with a Swagelok connector and optional vacuum gauge, and used with a PM probe to prevent light leakage²². Before measurement, the bubbler and Lucas cell were evacuated using a high-vacuum system. Exactly 70 mL of the water sample, pre-marked on the bubbler, was transferred via vacuum technique to maintain uniform volumes and minimize loss. A vacuum above the liquid allowed radon to escape as bubbles, which were then transferred to the pre-evacuated Lucas cell and left for 180 min to reach equilibrium with decay products. Finally, the cell was connected to a photomultiplier tube, and radon was counted using a programmable alpha counter. The count data were used to calculate the radon activity concentration in water using the following Eq. 2³.

$$C_{RnW} \text{ (Bq L}^{-1}\text{)} = \{6.97 \times 10^{-2} \times N\} / \{E \times V_w \times (1 - e^{-\lambda T'}) \times e^{-\lambda T}\} \quad (1)$$

Here, N represents the counts above background levels, V_w denotes the volume of water in L, E refers to the efficiency of the scintillation cell (74%), λ is the decay constant for radon (2.98×10^{-6} s), T indicates the counting delay from sampling to analysis (s), and T' represents the duration of the counting period (s). The USEPA has set a maximum contamination level (MCL) for radon in drinking water at 11.1 Bq L⁻¹ for communities without active radon mitigation programs²⁴. In contrast, the WHO recommends a reference level of 100 Bq L⁻¹ for radon in drinking water. If this concentration is exceeded, the WHO advises taking measures to reduce exposure²⁵.

Inhalation and ingestion doses of radon in water

In this study, seasonal measurements of radon in water are used to derive annual effective dose estimates. The calculations followed UNSCEAR/ICRP methodology^{26,27}, applying an indoor occupancy time (T) and an annual water consumption rate (C_w), as commonly adopted in other studies^{23,28,29}. The effective dose from inhalation and ingestion was then estimated using the following equation²⁶.

$$D_{inh} \text{ (} \mu \text{Sv y}^{-1} \text{)} = C_{RnW} \times R_{aw} \times F \times T_i \times DCF \quad (2)$$

$$D_{ing} \text{ (} \mu \text{Sv y}^{-1} \text{)} = C_{RnW} \times C_w \times K_D \quad (3)$$

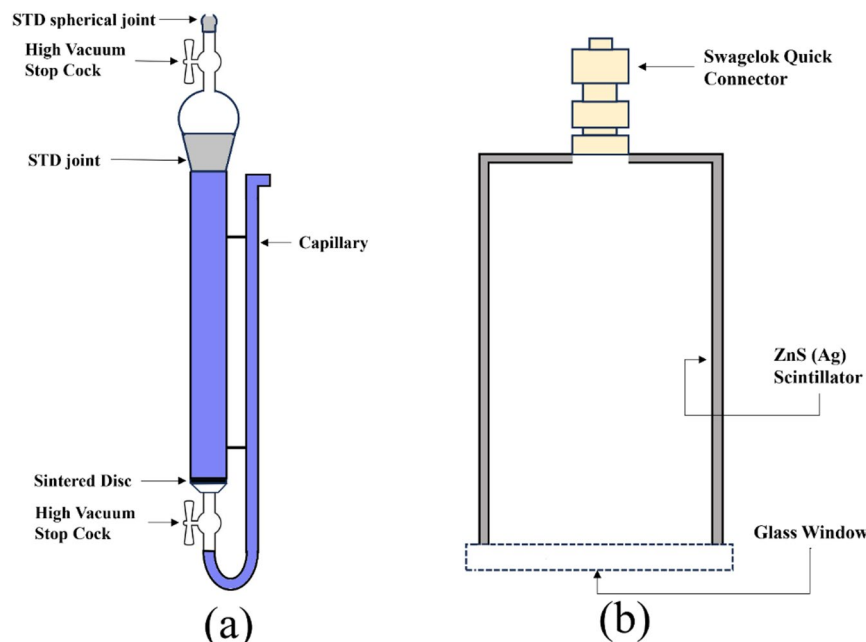


Fig. 2. Schematic representation of (a) radon bubbler, and (b) Lucas cell.

C_{RnW} is the concentration of radon in water, D_{inh} is the inhalation dose, and D_{ing} is the ingestion dose which calculated for two age groups: adults (Group 1) and children (Group 2). The total dose (D_{total}) represents the annual effective dose estimates, obtained as the sum of D_{inh} and D_{ing} . The Ingestion dose. R_{aw} is the ratio of radon in air to water (1.00E-04), F is the equilibrium factor between radon and its progenies (0.4), T_i is the mean indoor occupancy time per individual per year (7000 h y^{-1}), and DCF is the dose conversion factor (6.7E-06 mSv Bq^{-1} h^{-1} m^3 = 6.7 μ Sv Bq^{-1} h^{-1} L)³⁰. C_w is the weighted estimate of annual water consumption which varies globally. As per WHO²⁵, the average annual water consumption rate for adults is 730 L y^{-1} . For children, it is estimated to be two-thirds of this value²⁶, approximately 487 L y^{-1} . K_D is the ingestion dose coefficient (Adult: 6.9E-04 μ Sv Bq^{-1}). While ICRP²⁷ does not specify values for children, UNSCEAR^{26,31} reports indicate they may receive 1.5 to 2 times higher effective dose than adults due to physiological characteristics and greater tissue sensitivity. In this study, the dose coefficient for children was assumed to be twice that of adults (1.38E-03 μ Sv Bq^{-1}). According to WHO, the recommended combined annual effective doses from radon in drinking water via ingestion and inhalation is 100 μ Sv y^{-1} . The ICRP³² does not set a specific limit for drinking water alone but advises that total radon exposure from all sources should not exceed 1000 μ Sv y^{-1} .

Radon measurement in soil and assessment of alpha equivalent dose

For measurements of radon, radium and exhalation rates in soil samples, the sealed can technique was employed³³. About 1 kg of soil samples were collected from a depth of 10 cm from the surface²⁶ and immediately placed in zip-lock bags for transportation. To eliminate moisture and ensure consistent radon release, the samples were dried in an oven at 105 °C³⁴, ground into a fine powder and homogenized by passing through a 2 mm sieve. Exactly 250 g of the homogenized soil was transferred into a can, with an LR-115 Type-II detector positioned inside so that it remained suspended above the soil without direct contact. The can was securely sealed with adhesive tape to prevent radon escape or external air entry. To ensure uniform sample height, particle size, and density across all measurements, cans of identical volume from the same manufacturer were used, and all soil samples were sieved through the same 2 mm mesh, thereby minimizing variability and enhancing reliability. A schematic representation of the can used in the investigation is shown in Fig. 3. The detectors were exposed for 60 days, after which they were chemically etched in 2.5 N NaOH solution for 1 h to reveal alpha-particle tracks^{35,36}. To determine the background radon level, an empty container equipped with only an LR-115 detector was exposed for the same duration. The detector from this container was processed in the same way, and the resulting background track density was subtracted from each sample track count to obtain corrected values. Thus, the reported track density for each sample represents the background-corrected radon concentration.

Radon concentrations in soil

The revealed tracks were counted using an electronic spark counter and the result was expressed in tracks cm^{-2} . The track densities were subsequently converted into $Bq m^{-3}$ using the following equation³⁷.

$$C_{RnS} (Bq m^{-3}) = \rho / (t \times k) \quad (4)$$

Where, C_{RnS} is the radon concentrations in soil ($Bq m^{-3}$), ρ is the tracks obtained in LR-115 detectors (tracks cm^{-2}), t is the exposure period (60 d) and k is the sensitivity factor (0.021 tracks cm^{-2} per $Bq d m^{-3}$).

Radium content in soil

The effective radium content of the soil is calculated by using the following relation³⁸.

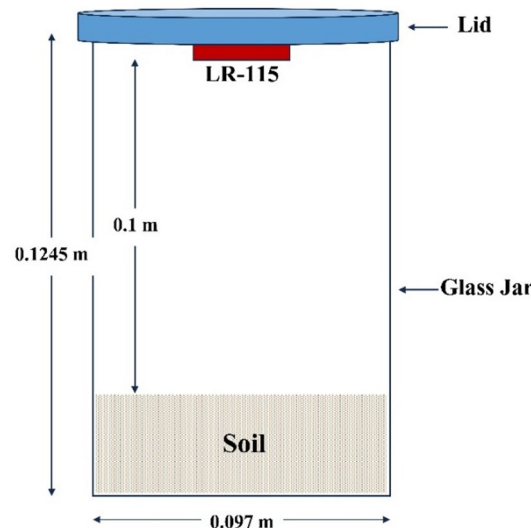


Fig. 3. Schematic representation of Sealed can technique for soil radon measurements.

$$C_{Ra} (Bq kg^{-1}) = (\rho \times H \times A_c) / (M \times T_e \times k) \quad (5)$$

Here, H is the distance between the top of the soil and the detector (0.1 m), A_c is the area of the cross section of the can (0.007391 m^2), M is the mass of the soil sample used (0.25 kg) and T_e is the effective exposure time and calculated as follows³⁹.

$$T_e = t + \tau (e^{-\lambda t} - 1) \quad (6)$$

Here, τ is the mean life of radon (5.5 d) and λ is the decay constant of radon (0.182 d^{-1}). The global average activity of radium content in soil is 35 Bq kg^{-1} and used as a reference value for radiological hazard assessment²⁶.

Radon exhalation rates

Calculating the radon exhalation rate from soil samples is crucial for determining the movement of radon gas into the dwellings, which directly impacts indoor air quality. The surface and the mass exhalation rates are calculated by using the following equations^{39, 40}.

$$E_s (Bq m^{-2} h^{-1}) = (C \times V_c \times \lambda) / (A_c \times T_e) \quad (7)$$

$$E_m (Bq kg^{-1} h^{-1}) = E_s \times (A_c / M) \quad (8)$$

Here, E_s represents the surface exhalation rate, E_m is the mass exhalation rate, C is the integrated radon exposure ($\text{Bq m}^{-3} \text{ h}$) obtained by multiplying C_{RnS} with the exposure period ($60 \text{ d} = 1440 \text{ h}$), λ is the decay constant of radon (0.00756 h^{-1}), V_c is the volume of the available space in the can, determined by subtracting the volume of the soil from the total volume of the can (0.00074 m^3), A_c is the area of cross section of the can (0.007391 m^2) and T_e is calculated from Eq. (6) in hour.

Alpha index and alpha equivalent dose

The health risk assessment related to radon exposure from soils are calculated by evaluating the alpha index (I_α) and the alpha equivalent dose (H_E). The alpha index is a radiological hazard index that helps assess the potential indoor radon exposure due to radium-226 in soil or building materials. It is calculated as follows^{41, 42}.

$$I_\alpha = C_{Ra} / 200 \quad (9)$$

Where C_{Ra} is the activity concentration of radium-226 in Bq kg^{-1} and 200 Bq kg^{-1} is a reference value, assuming a radon concentration of 200 Bq m^{-3} is the upper acceptable limit for indoor air. If $I_\alpha < 1$, radium levels are safe with expected indoor radon below 200 Bq m^{-3} , while $I_\alpha > 1$ indicates high radium levels that may raise indoor radon above 200 Bq m^{-3} , requiring mitigation.

The alpha equivalent dose from radon-226 in soil is key in assessing radon exposure in indoor air. The H_E is calculated using an empirical model applied to the volume of a standard reference room⁴³. The Commission of European Communities recommends a conversion factor of 1 Bq m^{-3} of radon corresponding to equivalent dose of 0.05 mSv y^{-1} , enabling alpha dose estimation using the specific activity of Ra-226 which under the assumption of secular equilibrium is equal to U-238^{44, 45}. The empirical model for calculating H_E in building materials and concrete was adapted and applied to soil samples. This approach is based on a linear relationship between the alpha equivalent dose and radium concentration, with the coefficient dependent on the material's bulk density. For the soil samples investigated in this work, a typical bulk density of 1600 kg m^{-3} was assumed, in accordance with standard UNSCEAR recommendations for soil density²⁶. Using the linear interpolation method based on the coefficients provided for materials with densities of 1750 kg m^{-3} and 2000 kg m^{-3} , the following equation of H_E (mSv y^{-1}) was derived for the soil samples.

$$H_E = (0.15 \times C_{Ra} \times f) + 0.45 \quad (10)$$

Where, C_{Ra} is the radium content in soil and f is the radon emanation factor which is a measure of the fraction of the radon atoms produced from the decay of radium in soil that escapes from the solid matrix into the pore spaces. It is a dimensionless parameter, generally varying between 0.05 and 0.7, with a mean value of approximately 0.2 observed in most type of soils²⁶.

Results and discussions

Ground water radon concentrations

The measured concentrations of radon in ground water samples (C_{RnW}) from the study area during summer and winter seasons are presented in Table 1.

The mean radon concentration in summer (57.87 Bq L^{-1}) is significantly higher than in winter (29.30 Bq L^{-1}). While the average radon concentrations measured in both summer and winter are below the WHO²⁵ guideline value of 100 Bq/L , they exceed the USEPA²⁴ maximum contaminant level of 11.1 Bq/L . During the summer season, all samples except S2 exceeded the USEPA limit, while sample S3 also surpassed the WHO guideline value. In winter, however, four samples (S2, S6, S7, and S14) were below the USEPA threshold limit. In addition, the high SD suggests moderate to high variability in radon concentrations among the sampling locations within the study area. The significant higher mean concentrations observed during the summer compared to the winter indicate notable seasonal fluctuations of radon in the groundwater. To determine the statistical significance of

Sample ID	Well depth (ft)	Sample locations		C _{RnW} (Bq L ⁻¹)	
		Latitude (°N)	Longitude (°E)	Summer	Winter
S1	70	26.10054	91.84827	12.50	34.04
S2	60	26.09746	91.85219	1.26	4.93
S3	190	26.09474	91.84866	128.47	27.28
S4	250	26.08963	91.84814	97.92	23.80
S5	120	26.08577	91.85404	94.48	51.05
S6	90	26.08484	91.84162	18.77	4.44
S7	80	26.07985	91.84635	66.97	5.17
S8	70	26.0844	91.82822	30.38	28.31
S9	80	26.08094	91.83472	97.50	35.11
S10	80	26.07668	91.82981	45.42	91.88
S11	140	26.07024	91.82917	61.77	45.64
S12	220	26.06179	91.82621	83.45	32.43
S13	140	26.06467	91.8163	19.24	30.64
S14	55	26.07392	91.81426	64.66	6.95
S15	85	26.07635	91.79995	45.29	17.84
Average				57.87	29.30
Standard deviation (SD)				36.19	21.89

Table 1. Measured values of radon concentrations in the study area.

the seasonal variation of radon concentrations a paired t-test (since measurements are from the same locations in both seasons) was performed using the null hypothesis⁴⁶ - H₀: There is no significant difference in seasonal radon concentrations and H₁: Radon concentration is significantly different between summer and winter season. Additionally, Cohen's d is calculated to determine whether there is a significant effect between the summer and winter datasets. According to Cohen⁴⁷, effect size can be categorized as follows: d < 0.2 = Small effect (Minimal practical significance), 0.2 ≤ d < 0.5 = Medium effect (Moderate practical significance), 0.5 ≤ d < 0.8 = Large effect (Substantial practical significance) and d ≥ 0.8 = Very large effect (Highly significant difference). The calculated t-value is 2.73 with p-value of 0.0163 indicating that the difference in seasonal radon concentrations is statistically significant ($p < 0.05$). This is also supported by the calculated value of Cohen's d (0.7948) indicating large effect in summer and winter radon concentrations. The seasonal variation of radon concentration in ground water is shown in Fig. 4. It is clear from the plot that radon concentrations have different shapes in summer and winter indicating seasonal variations. The KDE curve for summer is wider with higher values as compared to winter which is centered around lower values.

The seasonal trend of radon concentration in ground water obtained in the present investigation can be attributed to multiple geophysical, hydrogeological, and climatic factors. The summer season in the study area is typically characterized by heavy rainfall and high temperatures. Rising water tables during summer can lead to increased radon transport from the soil to the groundwater. Heavy rainfall in summer may enhances groundwater recharge, allowing water to percolate through radon-rich rock formations. This percolation process dissolves uranium-bearing minerals, increasing radon concentration in groundwater⁴⁸. The study area consists of granitoids (diorite, granodiorite, porphyritic granite) and Precambrian gneissic rocks, which are known for high uranium content^{49,50}. Rainwater percolates through fractures in granitic and gneissic formations, leading to radon accumulation in groundwater⁵¹. During rainfall, the water table rises, saturating the ground with water. This upward movement can displace radon-rich soil gas, causing an increase in radon concentrations in groundwater⁵². Some studies have also reported an increase in radon concentrations in groundwater during and after periods of heavy rainfall^{52,53}. In addition, increasing temperatures in summer can potentially lead to increased radon concentrations in groundwater. Higher soil temperatures in summer can increase the rate at which radon, a naturally occurring radioactive gas, emanates from the soil and rock into the surrounding air and groundwater⁵⁴. Although the overall trend in the present study indicates higher radon concentrations in groundwater during the summer season, a few sampling sites (S1, S10, and S13) exhibited relatively elevated radon levels in winter. This deviation may be reasonably explained by considering the complex geological and hydrogeological setting. The study area is underlain by Archaean Gneissic complex rocks, intrusive granites, and quartzites of the Precambrian Shillong Group, which are extensively fractured, fissured, and highly deformed. Such geological formations often create localized aquifer systems with variable fracture densities and permeability, influencing the movement, residence time, and accumulation of radon in groundwater⁵⁵. Previous studies have reported similar site-specific variations in radon concentrations, where micro-geological conditions, including fracture distribution, aquifer confinement, and recharge rates, can override regional seasonal trends at certain locations⁵⁶.

The overall mean concentration of radon for both the seasons in the study area is 43.59 Bq L⁻¹. A comparison of the radon concentrations in ground water obtained in the present investigation with the others recent reported values in the literature is shown in Table 2. The table indicates that the overall mean radon concentration in the present study area is comparable to, or in some cases slightly lower than the values reported in other regions. The

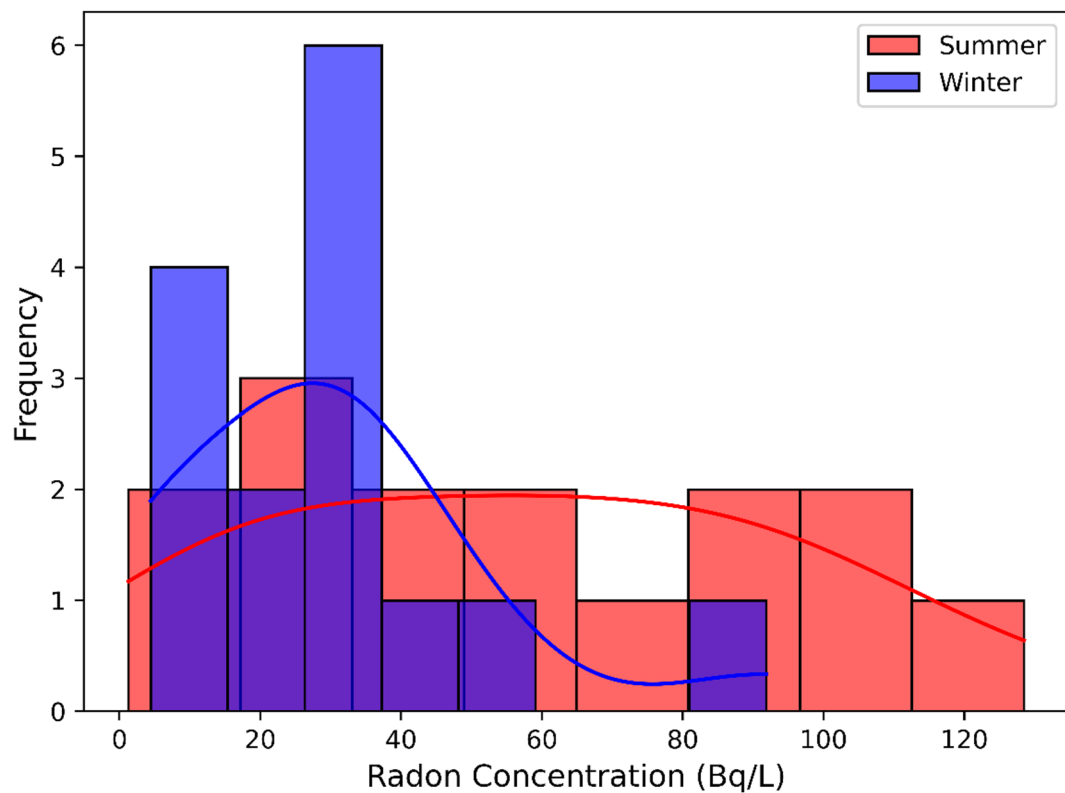


Fig. 4. Histogram with kernel density estimation (KDE) plot for seasonal radon variation in ground water.

Location	Mean radon concentrations (Bq L ⁻¹)	References
Bengaluru, India	38.3 ± 12.7	Deepika et al. ⁵⁷
Jammu & Kashmir, India	41.3 ± 1.0	Pandith et al. ⁵⁸
Baoji, China	41	Xinwei ⁵⁹
Bangalore, India	87	Prasad et al. ⁶⁰
Extremadura, Spain	111 ± 7 (all samples) 58 ± 3 (well water)	López and Sánchez ⁶¹
Rajasthan, India	113	Duggal et al. ²⁹
Juban District, Yemen	226.41 ± 62.39	Abdurabu et al. ⁶²
Yerevan city, Armenia	3.78 ± 0.84	Pyuskyulyan et al. ¹⁷
Al Jahra Governorate, Kuwait	9.01	Hassan et al. ⁶³
Raghunathpur municipality, West Bengal, India	49.78 ± 1.81	Mukherjee et al. ⁶⁴
The Anti-Atlas, the High Atlas and the Bahira areas, Morocco	52.99	Tairi et al. ⁶⁵
Er-Rachidia, Morocco	1.92	Said et al. ⁶⁶
Peshawar, Pakistan	12.0	Shah et al. ⁶⁷
Nagaland, India	1.82 ± 0.04	Jamir et al. ⁶⁸
Hafr Al Batin area, Saudi Arabia	1.16	Mamun & Alazmi ⁶⁹
Gadau, Bauchi State, Nigeria	38.3	Shu'aibu et al. ⁷⁰
Baridua Village, India	43.59	Present study

Table 2. Comparison of the radon concentrations in the present investigation with other reported values.

average radon concentrations in groundwater (for each sampling points) for both summer and winter seasons are calculated from Table 1, and a contour plot is generated (Fig. 5) to visualize the variations across the sampling locations. The calculated average value is further used to estimate the health risk due to ingestion and inhalation of radon in ground water.

From the plot, we observe that samples S3, S5, S9, and S10 exhibit high radon concentrations, ranging approximately between 65 and 80 Bq L⁻¹. Samples S9 and S10 have concentrations exceeding 50 Bq L⁻¹,

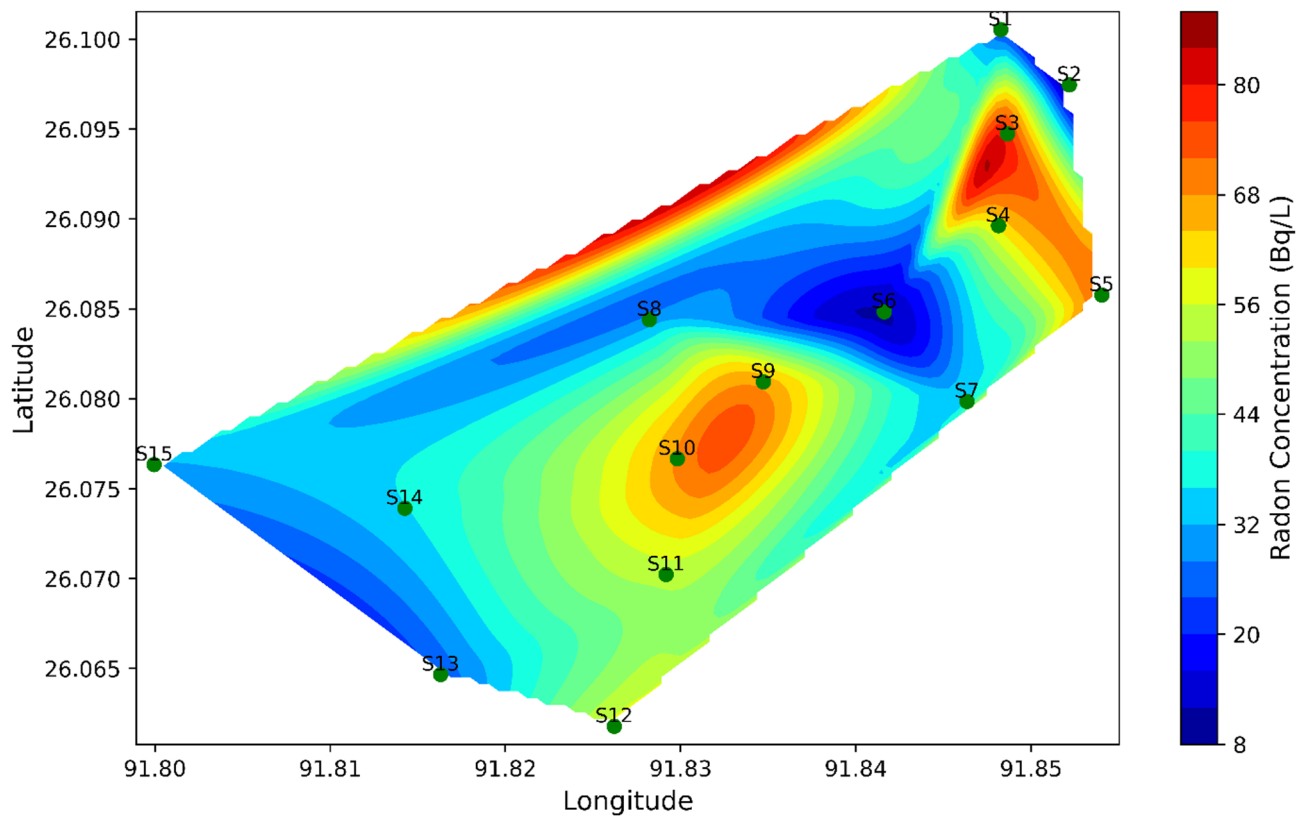


Fig. 5. Contour plot showing the distribution of radon (average of summer and winter values) in the ground water samples of the study area.

while the remaining samples have values below 40 Bq L^{-1} . The relationship between well depth and radon concentration in the study area appears non-linear. While samples S3 and S5 with relatively deeper wells (190 ft and 120 ft, respectively) show high radon levels ($65\text{--}80 \text{ Bq L}^{-1}$), samples S9 and S10 with shallower depths (80 ft) also exhibit elevated concentrations ($>50 \text{ Bq L}^{-1}$), suggesting that factors other than depth may influence radon levels in groundwater of the study area. Apart from well depth, radon concentration in groundwater may also be influenced by the geology of the study area, particularly the fractured and deformed Archaean gneissic rocks and granites, which enhance radon release. Additionally, the deep acidic soils and humid climate in the study area may facilitate radon migration and groundwater recharge through fissures and valleys. Although one sample exceeded the WHO limit during the summer (see Table 1), none of the samples surpassed the limit when considering the overall values (average of summer and winter). However, it is important to note that, except for sample S2, all samples exceeded the USEPA limit of 11.1 Bq L^{-1} .

Radiological dose assessment and Estimation of health risk from ground water samples

To assess the radiological health risk of radon, a health risk assessment is conducted for radon in water. Radon in water can be exposed to humans through two pathways: ingestion and inhalation. The corresponding doses from ingestion (D_{ing}) and inhalation (D_{inh}) are calculated using Eqs. (2) and (3) which is further used to evaluate the total dose ($D_{\text{total}}=D_{\text{ing}}+D_{\text{inh}}$). For the calculation of dose through the ingestion pathway, the population in the study area is classified into two groups based on annual water consumption: adults and children. The total dose is then estimated separately for each group. Table 3 provides the inhalation and ingestion doses of radon in water.

The mean annual effective dose estimates (D_{total}), derived from summer and winter radon data using UNSCEAR/ICRP recommendations, are $137.72 \mu\text{Sv y}^{-1}$ and $69.73 \mu\text{Sv y}^{-1}$ for adults, and $147.46 \mu\text{Sv y}^{-1}$ and $74.66 \mu\text{Sv y}^{-1}$ for children, respectively. During the summer season, the D_{total} for both adults and children exceeded the recommended limit of $100 \mu\text{Sv y}^{-1}$ set by UNSCEAR and WHO. However, in winter, the D_{total} remained below the recommended threshold for both age groups. The variation of ingestion, inhalation and the D_{total} during summer and winter seasons is shown in Fig. 6.

Figure 6 provides a comparative visualization of inhalation dose (D_{inh}), ingestion dose (D_{ing}), and total dose (D_{total}) of radon in groundwater for both adults and children across summer and winter seasons. It is evident from the figure that the doses are relatively higher in summer as compared to winter for all categories (inhalation, ingestion, and total dose). This seasonal difference reflects higher measured radon concentrations in groundwater samples during summer in the investigation area. In dose assessment, seasonal variation in water consumption was not considered, and constant annual ingestion rates were used for both seasons. Therefore, the observed difference in dose rates is attributed solely to seasonal variation in radon concentration. In summer, the mean inhalation dose is significantly higher than in winter. There is a wider spread (higher interquartile range,

Sample ID	Summer					Winter				
	D _{inh}	D _{ing}		D _{total}		D _{inh}	D _{ing}		D _{total}	
		Adult	Child	Adult	Child		Adult	Child	Adult	Child
S1	23.45	6.30	8.40	29.74	31.85	63.86	17.15	22.88	81.01	86.74
S2	2.36	0.63	0.85	2.99	3.20	9.25	2.48	3.32	11.74	12.57
S3	241.01	64.71	86.34	305.71	327.34	51.18	13.74	18.33	64.92	69.51
S4	183.71	49.32	65.81	233.03	249.52	44.65	11.99	16.00	56.64	60.64
S5	177.24	47.59	63.49	224.83	240.73	95.78	25.72	34.31	121.49	130.09
S6	35.22	9.46	12.62	44.68	47.84	8.32	2.23	2.98	10.56	11.30
S7	125.64	33.73	45.01	159.37	170.64	9.69	2.60	3.47	12.29	13.16
S8	56.99	15.30	20.42	72.29	77.40	53.11	14.26	19.03	67.37	72.13
S9	182.90	49.11	65.52	232.01	248.42	65.86	17.68	23.59	83.55	89.46
S10	85.21	22.88	30.53	108.09	115.74	172.37	46.28	61.75	218.65	234.12
S11	115.89	31.12	41.52	147.00	157.40	85.61	22.99	30.67	108.60	116.29
S12	156.55	42.03	56.08	198.59	212.64	60.84	16.34	21.80	77.18	82.64
S13	36.10	9.69	12.93	45.79	49.03	57.47	15.43	20.59	72.90	78.06
S14	121.31	32.57	43.46	153.88	164.77	13.03	3.50	4.67	16.53	17.70
S15	84.96	22.81	30.44	107.77	115.39	33.47	8.99	11.99	42.46	45.46

Table 3. Calculated values of inhalation, ingestion and total doses for every sample (Values are in $\mu\text{Sv y}^{-1}$).

IQR) in summer, indicating greater variability in radon exposure through inhalation. Some outliers in winter suggest that a few locations might still have relatively high radon concentrations despite the seasonal reduction. Ingestion doses for both adults and children remain lower than inhalation doses in both seasons. This outcome is expected, as the dose model follows the WHO and UNSCEAR assumptions, which identify inhalation of radon released into indoor air from water as the dominant exposure pathway, with ingestion contributing comparatively less to total dose. The IQR and median values indicate that the variability is lower in ingestion compared to inhalation, meaning that groundwater radon ingestion is more consistent across the study area. Inhalation doses from radon in drinking water are generally higher than ingestion doses, as radon released into the air is inhaled, directly exposing the respiratory tract, whereas ingestion primarily affects the gastrointestinal tract⁷¹. When water containing radon is used for activities like showering or washing dishes, radon gas can escape and enter the indoor air. Breathing in this gas can expose the lungs to radiation. This released radon can then be inhaled, leading to radiation exposure of the lungs²⁵. Radon can be ingested by drinking contaminated water, but the radiation exposure from this route is generally lower than that from inhalation. The total dose follows the same trend as inhalation and ingestion, showing higher values in summer than in winter. The median and mean values for summer exceed $100 \mu\text{Sv y}^{-1}$, the recommended annual dose limit by UNSCEAR and WHO. This indicates potential health risks during summer. In winter, although the doses decrease, there are a few outliers where some samples still show elevated radon levels. The box plot shows that children receive a slightly higher total dose than adults in both seasons. This outcome is expected under the adopted age-dependent dose conversion factors that are higher for children. Seasonal variations in groundwater radon levels lead to higher doses in summer, emphasizing the need for monitoring, especially during peak seasons. Children receive higher doses than adults, making them a vulnerable group that requires risk mitigation measures. Since inhalation is the main contributor to total dose, proper indoor ventilation and aeration of drinking water are essential. Although winter doses are lower, some sites still show high levels, highlighting the need for continuous year-round monitoring.

The stochastic health risk assessment was performed using a Monte Carlo Simulation (MCS) to estimate the total effective dose due to radon exposure through ingestion and inhalation pathways. The simulation was implemented in Python 3 using average radon data from both seasons rather than analysing each season separately. This approach incorporated uncertainties in exposure parameters for both adults and children by randomly sampling input variables from their probability distributions and computing inhalation and ingestion doses in each iteration based on standard dose equations. In this model, lifestyle-related exposure assumptions were based on UNSCEAR and ICRP recommendations^{4,27}, reflecting typical living conditions in the study area. The indoor occupancy time (T_i) was assumed to be 7000 h y^{-1} , representing a predominantly indoor lifestyle. The radon concentration in water (C_{RwW}) was modelled using a lognormal distribution derived from experimentally measured mean and standard deviation values. Annual water ingestion rates (C_w) were modelled as normally distributed, with a mean of 730 L y^{-1} for adults and 487 L y^{-1} for children. The mean annual ingestion rates for adults and children, were used to model intake variability via a lognormal distribution under three assumed coefficients of variation (CV = 20%, 25%, and 30%)²². For each CV, Monte Carlo simulations were performed, and distribution characteristics (median, 95th percentile, and spread) were compared to assess sensitivity. Sensitivity analysis showed CV = 20% underestimated variability, CV = 30% overestimated extremes, and CV = 25% gave a balanced spread with the median close to the mean and realistic upper-tail values, making it the most suitable for both groups. With a CV of 0.25, the estimated standard deviation was 182.5 L y^{-1} for adults and 121.75 L y^{-1} for children. Other parameters, including the ratio of radon in air to water ($R_{aw} = 1.00 \text{E-04}$), the equilibrium factor ($F = 0.4$), and the dose conversion factors for ingestion and inhalation, were fixed at values recommended by ICRP and UNSCEAR.

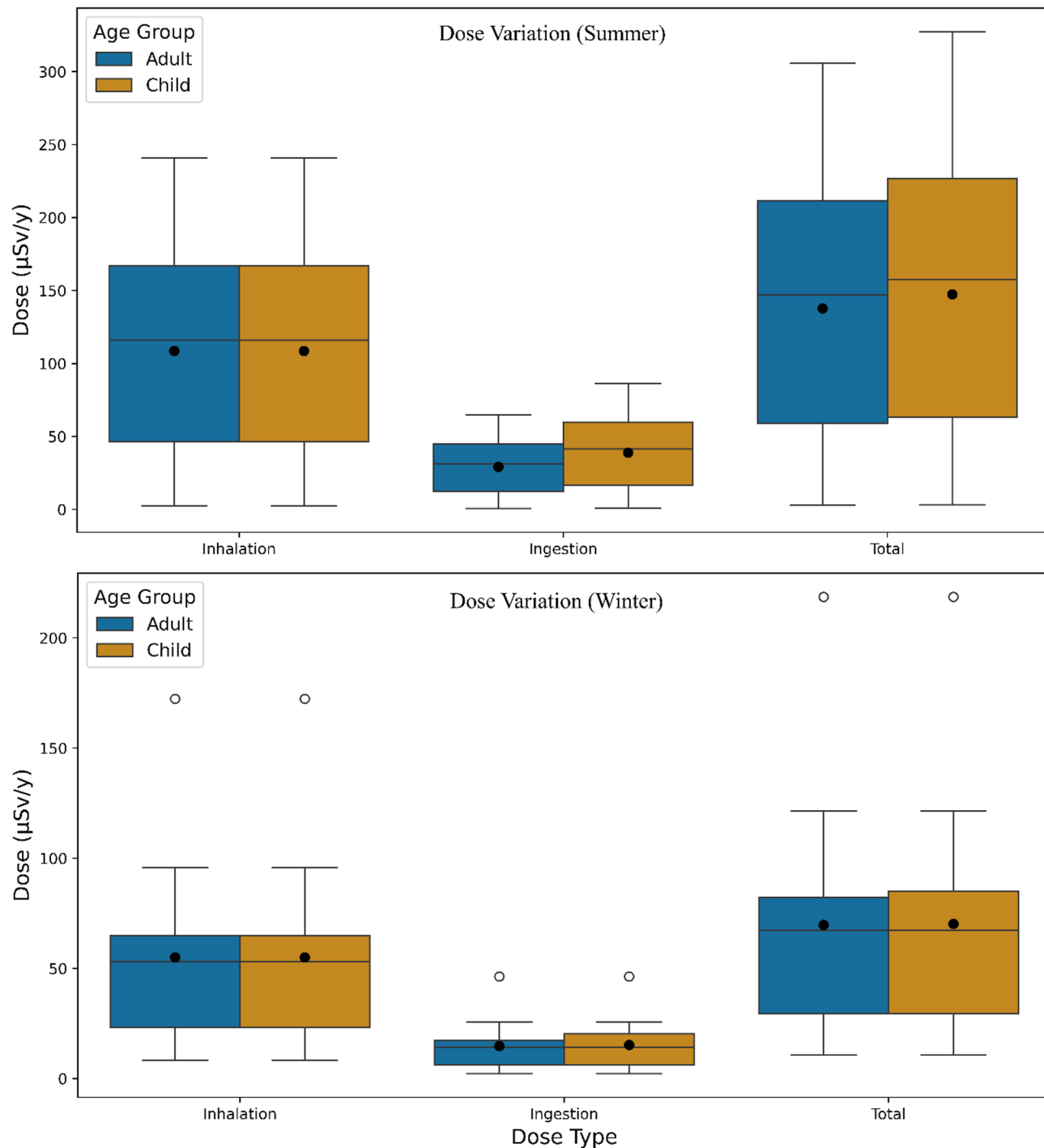


Fig. 6. Box plot showing the variation of doses during the monitoring period.

A total of 100,000 simulation iterations were carried out to produce stable dose distributions for each age group. In each iteration, inhalation and ingestion doses were calculated using the sampled and fixed parameter values, and the annual effective dose derived from summer and winter data was estimated by summing both pathways. The resulting distributions were analysed to determine the mean, median, and the probability of exceeding the risk threshold of $100 \mu\text{Sv y}^{-1}$. The results of the Monte Carlo simulation indicate distinct exposure patterns for adults and children. As shown in Fig. 7, the mean and median values of doses for adults were $103.49 \mu\text{Sv y}^{-1}$ and $91.78 \mu\text{Sv y}^{-1}$, respectively, with a health risk probability of 43.19%. However, Fig. 8 depicts a higher risk for children, with a mean of $111 \mu\text{Sv y}^{-1}$, a median of $98.66 \mu\text{Sv y}^{-1}$, and a corresponding health risk probability of 48.91%. This outcome is expected under the adopted age-specific parameterization, in which children have higher dose conversion factors and higher water intake per unit body mass than adults. These

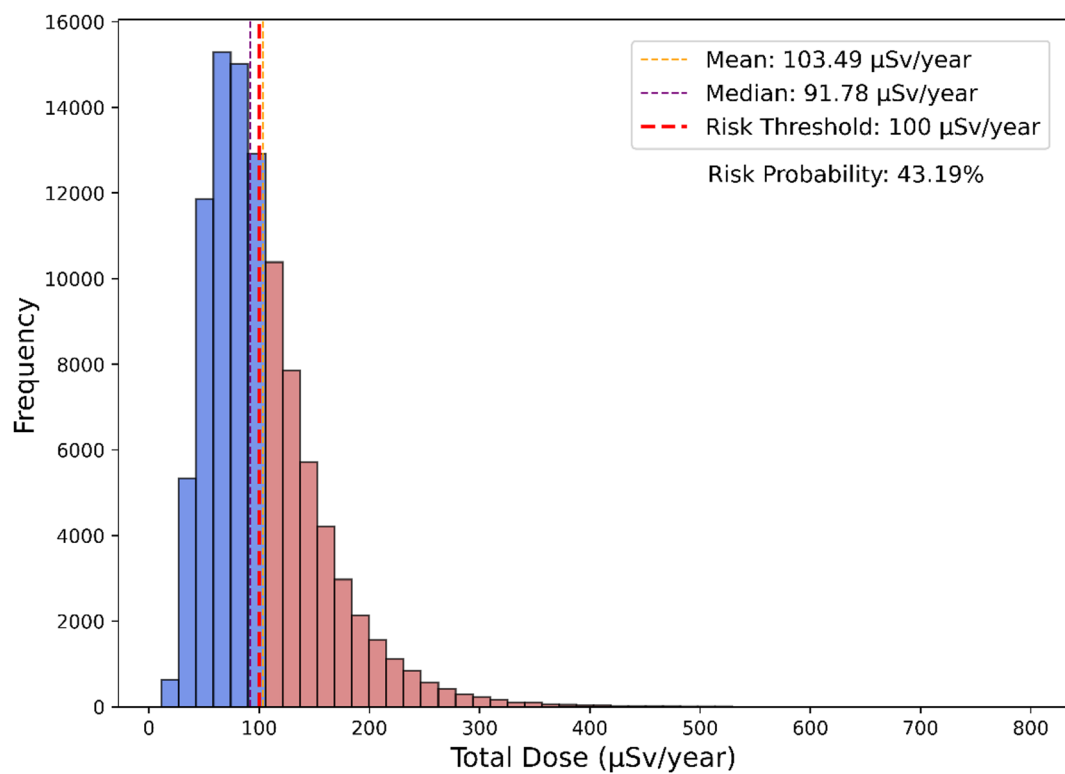


Fig. 7. Results of MCS for adult indicating the risk probability of exceeding the threshold value.

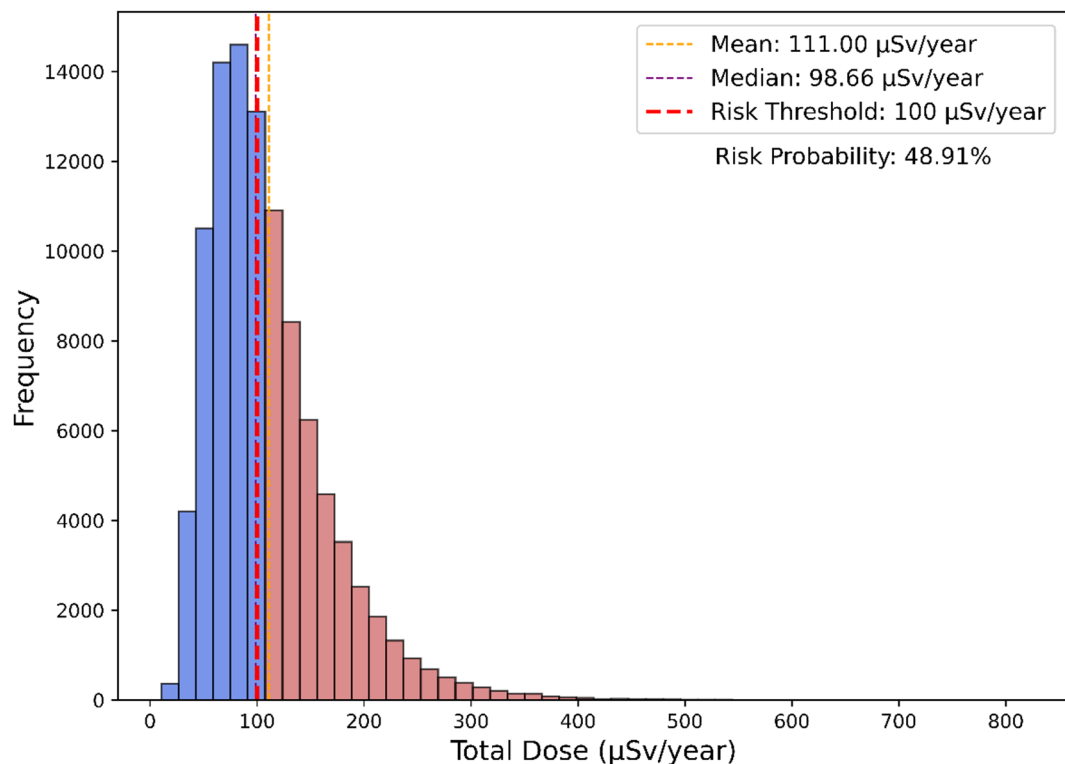


Fig. 8. Results of MCS for child indicating the risk probability of exceeding the threshold value.

findings reinforce the need for targeted risk mitigation strategies, particularly in regions where groundwater serves as the primary drinking water source.

Soil radioactivity measurements

Soil radon concentration, soil radium content, surface exhalation rate, and mass exhalation rate of radon in the study area were calculated using Eqs. (4), (5), (7), and (8). The results for both seasons are presented in Fig. 9.

The soil radon concentrations (C_{RnS}) ranged from 406.35 to 1721.43 Bq m⁻³ collected during summer and 320.63 to 1626.98 Bq m⁻³ collected during winter. The average concentration recorded in summer was 938.57 Bq m⁻³ while in winter it was 777.14 Bq m⁻³. Radon levels can fluctuate significantly depending on factors like soil type, depth, and geological context. Radon concentrations in typical soils can range from 4000 to 40,000 Bq m⁻³⁷³. Radium concentration (C_{Ra}) varied from 1.32 to 5.60 Bq kg⁻¹ in summer and 1.04 to 5.30 Bq kg⁻¹ in winter, with mean values of 3.05 Bq kg⁻¹ and 2.53 Bq kg⁻¹, respectively. These values are within the global average value (35 Bq kg⁻¹) reported for soil radium content by UNSCEAR²⁶. The overall variation in soil radium remains small indicating that soil radium remains stable with less seasonal variation. Radium-226 is a solid, long-lived radionuclide with a half-life of about 1600 years. It is part of the mineral matrix in soil, typically bound to clay minerals, organic matter, or incorporated into rock grains. Because of this, its concentration in soil stays relatively stable over time, unless there is major geological disturbance, erosion, or anthropogenic activities like mining or waste dumping²⁶. The surface exhalation rates (E_s) ranged from 0.34 to 1.43 Bq m⁻² h⁻¹ in summer and 0.27 to 1.36 Bq m⁻² h⁻¹ in winter. Similarly, the mass exhalation rates (E_m) varied between 0.010 and 0.042 Bq kg⁻¹ h⁻¹ in summer and 0.008 to 0.040 Bq kg⁻¹ h⁻¹ in winter. The average E_s was found to be 0.78 Bq m⁻² h⁻¹ in summer and 0.65 Bq m⁻² h⁻¹ in winter, while the average value of E_m was 0.023 Bq kg⁻¹ h⁻¹ in summer and 0.019 Bq kg⁻¹ h⁻¹ in winter. The surface exhalation rates and the mass exhalation rates remained below the world average values of 57.6 Bq m⁻² h⁻¹ and 0.034 Bq kg⁻¹ h⁻¹^{26,74}.

From the observations, a slight difference is noted in the average values of soil radon, soil radium, and exhalation rates. However, this difference is minimal and cannot be directly attributed to seasonal variations. In addition, as the measurements were carried out using the sealed can technique, which involved drying the soil samples under uniform laboratory conditions. Slightly higher concentrations were generally observed during summer compared to winter, except at sites S4, S5, S8, and S10. The observed variations across different sampling locations are likely due to the geological heterogeneity of the study area, Ri-Bhoi district. The Shillong Plateau, which encompasses Ri-Bhoi, is characterized by complex geology comprising granite, gneiss, and structurally disturbed zones such as the Kopili Fault⁷⁵. A recent study reported significant differences in radon exhalation rates from granite, gneiss, and soil samples collected within a few km of each other near the Kopili Fault⁷⁶. Additionally, the ability of radon to escape from soil varies with factors such as porosity, density, and grain size, even after drying and sieving. In Ri-Bhoi district, agricultural soils, hilltop soils, and inter-hill valley soils differ in texture and density⁷⁷, which may further contribute to the variability in radon exhalation rates.

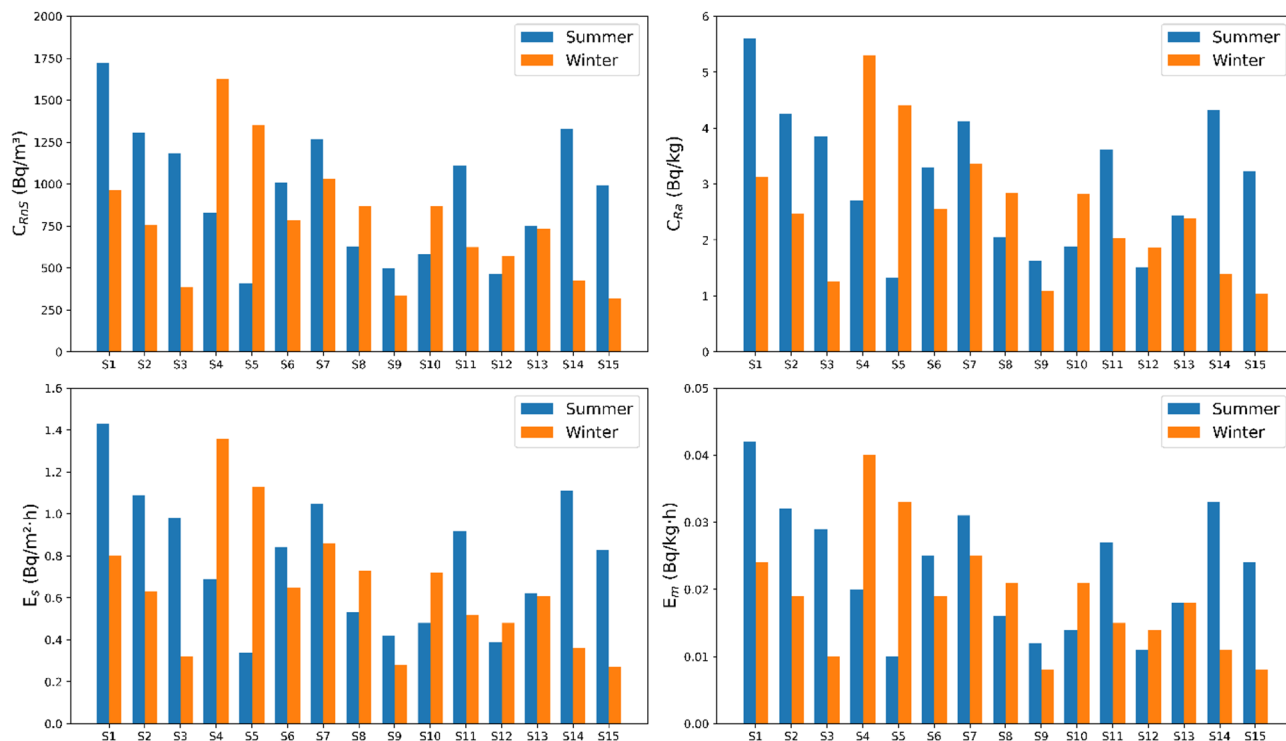


Fig. 9. Variation of radon parameters in soil across the collected samples.

Alpha equivalent dose and Estimation of health risk due to radon in soil

The alpha index (I_{α}) and the alpha equivalent dose (H_E) are calculated by using Eqs. (9) and (10). Assessing the alpha index of radon in soil is essential for evaluating potential health risks linked to radon exposure, especially the risk of lung cancer. Radon, a naturally occurring radioactive gas, decays into alpha-emitting isotopes that can harm lung tissue when inhaled. The alpha index quantifies this risk by accounting for the energy and concentration of alpha particles emitted by radon decay products^{78,79}. Of the total hazard associated with uranium, around 98.5% of the health risk is attributed to radium and its progeny^{44,45}. Consequently, the effective dose is determined by evaluating the alpha equivalent dose resulting from radium content in the soil. Table 4 displays the computed I_{α} and H_E values for all samples collected in both seasons.

The alpha index across all samples ranged from 0.007 to 0.028 during summer and from 0.005 to 0.026 during winter. The highest value was observed in sample S1 (0.028 in summer) and S4 (0.026 in winter). All samples recorded values well below the limiting value of 1 in both seasons, indicating minimal radiological risk from radon in the soil. The alpha equivalent dose varied between 0.498 and 0.652 mSv y^{-1} in summer and between 0.488 and 0.641 mSv y^{-1} in winter. The highest dose was observed in sample S1 during summer (0.652 mSv/y) and in sample S4 during winter (0.641 mSv y^{-1}). Again, all samples showed values below the safety limit of 1 mSv y^{-1} , suggesting that the health risk due to alpha radiation exposure from soil radon remains within acceptable limits^{44,80}.

Radon can infiltrate indoor air from sources such as soil, building materials, and outdoor air. However, the main concern lies in the release of radon from the decay of radium present in soil, which can significantly elevate indoor radon levels and, in turn, increase radiation doses. Building materials can also contribute to indoor radon levels and associated radiation doses, although their contribution is typically lower compared to that from soil^{81,82}. There are very limited number of studies conducted in the state of Meghalaya relating to the measurements of radon exhalation rates in building materials. A recent study conducted in the Jowai region of Meghalaya assessed the radon and thoron exhalation rates from commonly used building materials in the state. The findings indicated that these materials do not pose any significant health risk from radiation exposure, suggesting they are safe for use in residential construction in the region⁸³. In the present investigation, the contribution of building materials to alpha equivalent doses remains uncertain, as these materials were not analysed. However, to facilitate a stochastic risk assessment, we have assumed a worst-case scenario in which building materials are assigned an equal contribution to the alpha equivalent doses for each sample. For example, a worst-case scenario was considered by assuming that the radium content of the building materials is identical to that of the soil in the study area. The maximum radium concentration in soil was found to be 5.60 Bq kg^{-1} , with a standard deviation of 1.225 Bq kg^{-1} . This same maximum value was assigned to the building materials. Therefore, the combined maximum radium concentration used in the Monte Carlo simulation was set at 11.2 Bq kg^{-1} , accounting for contributions from both soil and building materials. The standard deviation for the new maximum value was estimated by assuming a constant coefficient of variation, meaning that the SD changes in direct proportion to the maximum value. Accordingly, the SD corresponding to a maximum value of 11.2 Bq kg^{-1} was calculated to be 2.45 Bq kg^{-1} . Based on this assumption, a stochastic assessment of alpha equivalent dose was carried out using a Monte Carlo Simulation (MCS) technique to account for the variability in soil radium concentrations. A total of 100,000 simulation iterations were performed to generate a stable distribution of possible dose outcomes. The concentration of radium in soil (C_{Ra}) was modelled using a lognormal distribution, characterized by a maximum value of 11.2 Bq kg^{-1} and a standard deviation of 2.45 Bq kg^{-1} . All other parameters in the dose equation (Eq. 10), including the emanation factor ($f = 0.2$) and the constant dose contribution from other environmental sources (0.45 mSv y^{-1}), were treated as fixed values. In each iteration, a value of C_{Ra} was randomly sampled

Sample ID	Alpha index		Alpha equivalent dose (mSv y^{-1})	
	Summer	Winter	Summer	Winter
S1	0.028	0.016	0.652	0.563
S2	0.021	0.012	0.603	0.539
S3	0.019	0.006	0.588	0.495
S4	0.013	0.026	0.547	0.641
S5	0.007	0.022	0.498	0.609
S6	0.016	0.013	0.568	0.542
S7	0.021	0.017	0.598	0.571
S8	0.010	0.014	0.524	0.552
S9	0.008	0.005	0.509	0.489
S10	0.009	0.014	0.518	0.552
S11	0.018	0.010	0.580	0.489
S12	0.008	0.009	0.504	0.517
S13	0.012	0.012	0.538	0.536
S14	0.022	0.007	0.605	0.500
S15	0.016	0.005	0.566	0.488

Table 4. Calculated values of alpha index and effective alpha dose.

from its distribution and used to compute the corresponding alpha equivalent dose (H_E) using Eq. (10). The resulting distribution of the dose values was then analysed to determine the mean, median, and range, and to estimate the probability of exceeding the recommended dose threshold of 1 mSv y^{-1} . This stochastic approach enabled a more realistic assessment of radiological risk associated with alpha-emitting radionuclides in soil by incorporating the natural variability observed in measured radium concentrations. The output of the MCS, as shown in Fig. 10, represents the probability distribution of the alpha equivalent dose. The histogram reflects the results of a large number of iterations (100,000), capturing the randomness and variability in dose estimates due to the inherent uncertainties in input parameters. The mean and median values (0.79 and 0.79 mSv y^{-1}) are aligned, indicating a symmetric distribution around the central value. This suggests that, in most scenarios, the alpha equivalent dose remains well below the threshold of 1.0 mSv y^{-1} , which is the reference limit for public exposure recommended by regulatory bodies^{26,80,84}. The simulated doses range from 0.59 to 1.26 mSv y^{-1} . The upper tail of the distribution extends slightly beyond 1.0 mSv y^{-1} , signifying a non-negligible probability of exceeding the regulatory limit. The simulation quantifies a 0.73% probability that the dose exceeds 1.0 mSv y^{-1} . This indicates that the likelihood of the alpha equivalent dose exceeding the recommended public dose limit is minimal under the simulated conditions, suggesting that the potential radiological health risk in the study area remains within acceptable safety limits for the majority of cases.

Soil radon vs. water radon

The relationship between soil radon (C_{RnS}) and water radon (C_{RnW}) was evaluated using the average values obtained from both summer and winter measurements. The scatter plot illustrating the correlation between soil and water radon concentrations is presented in Fig. 11. The scatter plot shows a widely spread set of points without a clear upward or downward trend. A few samples, such as S1 and S4, have high soil radon but moderate water radon, while others, like S3 and S5, have high water radon but only moderate soil radon. The Pearson correlation coefficient of -0.34 suggests a weak negative correlation between radon concentrations in water and soil. The p -value of 0.215 is greater than the conventional significance threshold (0.05). This indicates no statistically significant correlation. In other words, we do not have sufficient evidence to reject the null hypothesis of no correlation. The Spearman rank correlation, which tests for a monotonic relationship (not necessarily linear), also shows a weak negative correlation ($\rho = -0.32$) with a p -value of 0.237 , again indicating no significant relationship.

Although radon is a noble gas that originates from the radioactive decay of radium in soil and rocks, its migration into groundwater is governed by complex geochemical and hydrogeological processes. Radon transport from soil to water is highly dependent on geological and hydrogeological conditions, including the type of aquifer, soil permeability, porosity, and presence of fractures or faults. In heterogeneous formations, radon may bypass certain soil zones or accumulate in isolated pockets, disrupting any linear soil-water relationship⁸⁵. In addition, radon entry into groundwater varies with the depth of the water table. Shallow aquifers typically

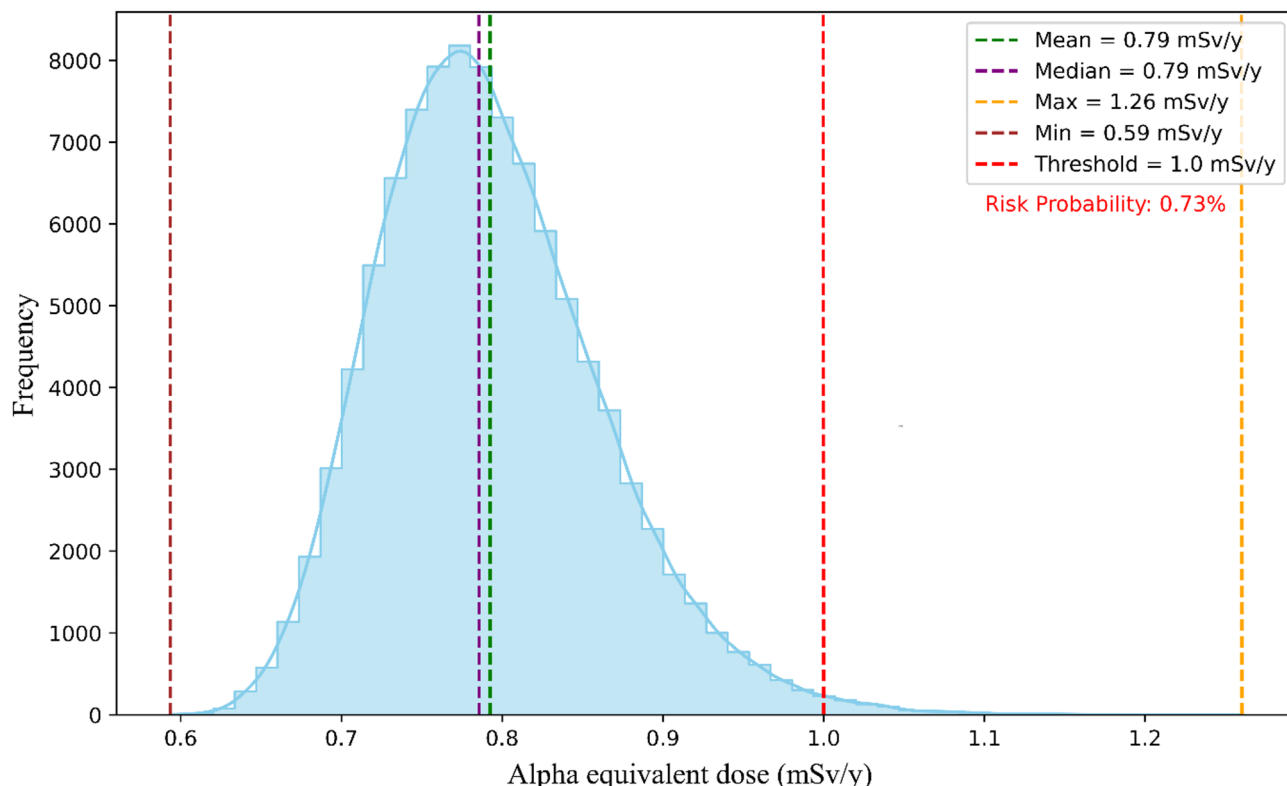


Fig. 10. Results of MCS for estimating the risk probability of alpha equivalent dose due to radon in soil.

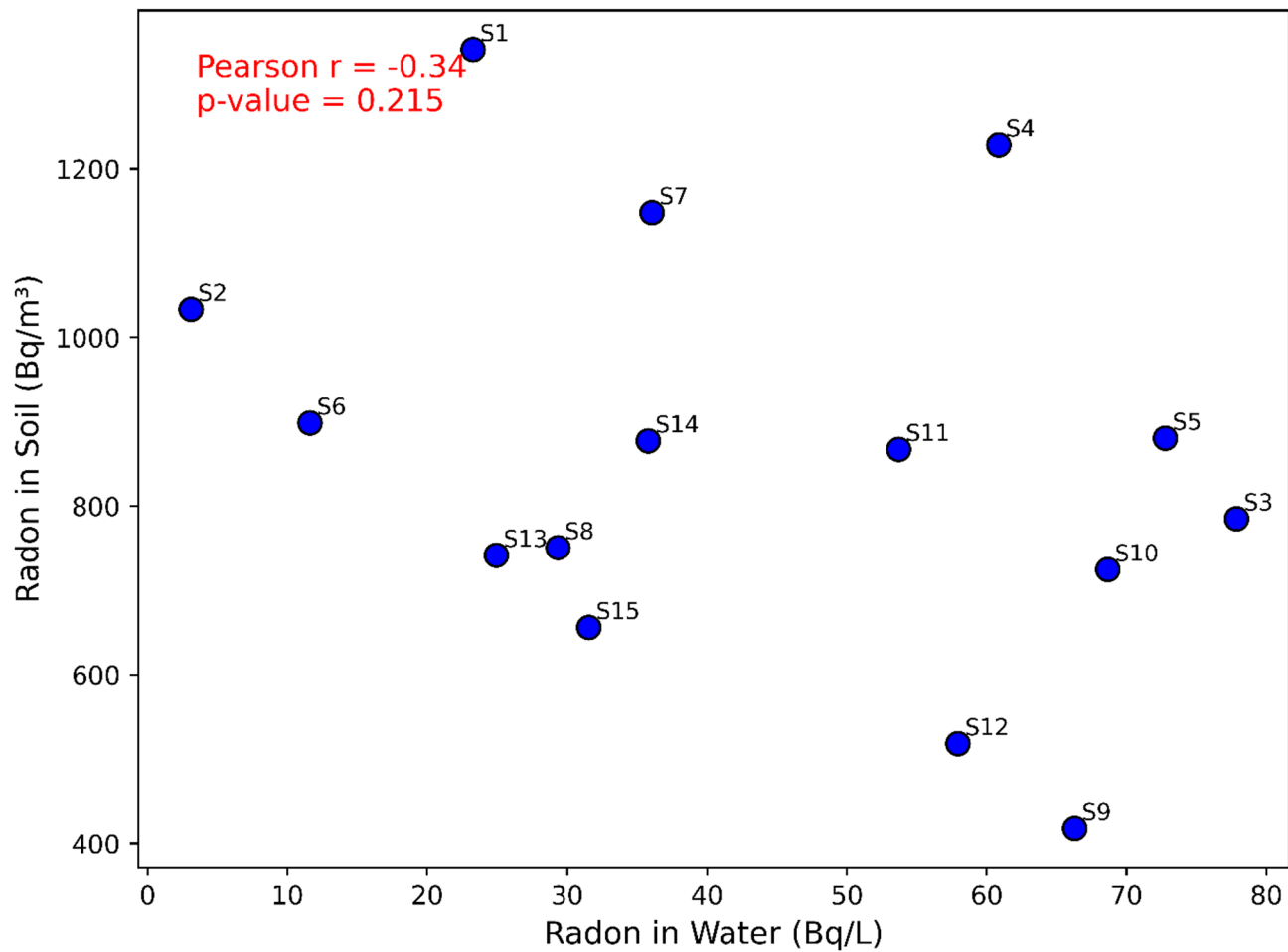


Fig. 11. Scatter plot of radon concentrations in water and soil.

show a stronger link between soil and water radon, while deeper aquifers may have less direct interaction with overlying soil gas due to radon decay before it reaches the aquifer⁵⁵. Together, these factors underscore that radon transport is not governed solely by soil concentrations but is a function of multi-factorial environmental dynamics. Therefore, mapping the geological features of the study area and analysing key hydrogeological parameters (such as soil type and water table depth) alongside radon measurements are essential for establishing a clearer understanding of the relationship between soil and water radon. We recommend conducting further studies that incorporate these parameters to better clarify the multifactorial influences on radon distribution.

Method validation and regional risk mitigation strategies

While the emanometry method involving grab sampling is relatively time consuming and labour intensive, it is a well established and reliable technique for detecting radon in water. Moreover, it is cost-effective and accessible, making it suitable for large scale surveys in resource-limited settings. The grab sampling approach, though straightforward and precise, presents challenges, especially in minimizing radon loss during sample collection and handling⁸⁶. To address this, strict protocols were followed: water was first pumped into a 10 L bucket, and sampling bottles were filled while submerged to avoid aeration, sealed underwater with airtight caps, and immediately transported to the laboratory for analysis. The laboratory setup included a radon bubbler with leak-proof couplings and a high-voltage vacuum pump connected to a Lucas cell, ensuring efficient radon extraction and minimal loss. Despite the availability of advanced instruments like RAD7 and AlphaGuard, the emanometry technique remains a reliable alternative when conducted with due diligence as reported by other investigators^{21,23}. The choice of LR-115 in the present study for reliable and efficient measurement of radon concentration in soil was guided by their practical advantages in field applications. While the CR-39 is globally recognized for its higher sensitivity and resolution, LR-115 has certain practical advantages in environmental monitoring applications. A comparative study conducted by Dwaikat et al. using CR-39 and LR-115 detectors under identical environmental conditions reported a strong correlation ($R = 0.99$) between the radon concentrations measured by both detector types, demonstrating that LR-115 can provide performance comparable to CR-39 in practical applications⁸⁷. However, the detector time efficiency (DTE) of LR-115 was found to be higher than that of CR-39. This suggests that LR-115 is not only efficient but also more sensitive for radon detection in this context. Additionally, LR-115 offers the practical advantage of selective sensitivity: it does

not record alpha particles from surface-deposited radon progeny when etched for short durations, reducing the risk of overestimation⁸⁸.

Based on the findings and considering the complex geological setting of the study area, the authors recommend the implementation of region-specific public health and regulatory measures. Given that groundwater radon concentrations exceeded the USEPA limit in most samples, particularly in summer, authorities should prioritize seasonal monitoring of radon levels in drinking water sources, especially during the summer months when concentration peaks are observed. For areas showing elevated risk probabilities, particularly for children as indicated by Monte Carlo simulations (48.91% exceedance), mitigation strategies such as aeration of water before household use and promotion of alternative low radon sources during high-risk periods are recommended. Moreover, awareness programs should be launched to educate communities about the health risks of radon exposure and encourage periodic testing of indoor air and drinking water. Although the alpha equivalent dose from soil radon remains largely within safe limits, future building codes in the region should consider radon resistant construction practices, since worst case scenario modelling shows a non-zero exceedance risk. Public health agencies are also encouraged to invest in long term, in-situ radon monitoring infrastructure and incorporate building material analysis into future exposure assessments for comprehensive regulation and improved risk mitigation.

Conclusion

This study found that while average groundwater radon concentrations were below the WHO guideline, most samples, particularly in summer exceeded the USEPA limit. Radiological risk assessment showed that the mean total doses during summer exceeded the UNSCEAR/WHO limits for both adults and children. Monte Carlo simulations indicated a 48.91% probability of children exceeding the dose threshold, highlighting their greater vulnerability. Soil radon, radium, and exhalation rates showed only minor seasonal differences, with alpha equivalent doses from soil remaining within safe limits and a 0.73% exceedance probability under a worst-case scenario. No significant correlation between soil and water radon was observed, suggesting that geological, hydrogeological, and climatic factors influence radon transport in the area. Future work should use active in-situ monitoring with concurrent meteorological measurements to capture short-term variations, and include data from additional seasons such as dry summer and spring for better understanding of annual trends. While MCS results for soil indicate a low probability of exceeding safety limits, continued monitoring and inclusion of actual building material radium levels and detailed indoor exposure parameters in future assessments are recommended to ensure long-term public safety.

Data availability

The data generated in this research are available within the manuscript in the form of tables and figures.

Received: 13 May 2025; Accepted: 3 October 2025

Published online: 10 November 2025

References

1. Nunes, L. J. R., Curado, A. & Lopes, S. I. The relationship between radon and geology: Sources, transport and indoor accumulation. *Appl. Sci.* **13**, 7460 (2023).
2. Zhang, S. et al. Potential radon risk in permafrost regions of the Northern hemisphere under climate change: A review. *Earth Sci. Rev.* **250**, 104684 (2024).
3. World Health Organization. *WHO Handbook on Indoor Radon: A Public Health Perspective* (World Health Organization, 2009).
4. UNSCEAR. *Sources, Effects and Risks of Ionizing Radiation, United Nations Scientific Committee on the Effects of Atomic Radiation, UNSCEAR 2019 Report To the General Assembly, with Scientific Annexes* (United Nations, 2020).
5. CGWB. Ground Water Information Booklet, Ri-Bhoi District, Meghalaya: Technical Report Series D. (2013). https://www.cgwb.gov.in/old_website/District_Profile/Meghalaya/Ri%20Bhoi.pdf
6. Chopra, R., Panigrahi, B., Yadav, R. & Joshi, G. B. Sandstone-type uranium resource potential of Mahadev Basin, Meghalaya, India. *Explor. Res. At. Miner.* **25**, 175–185 (2015).
7. MGD. Minerals of Meghalaya: Directorate of Mineral Resources, Department of Mining and Geology, Government of Meghalaya. (2022). <https://megdmg.gov.in/minerals.html>
8. Dwivedi, K. K., Mishra, R. & Tripathy, S. P. An extensive indoor 222Rn/220Rn monitoring in North-East India. *Radiat. Meas.* **40**, 621–624 (2005).
9. War, S. A., Nongkynrih, P., Khathing, D. T. & Longwai, P. S. Assessment of indoor radiation level in the environs of the uranium deposit area of West Khasi Hills District, Meghalaya, India. *J. Environ. Radioact.* **100**, 965–969 (2009).
10. Khardewasaw, A., Maibam, D., Sharma, Y. & Saxena, A. Studies on indoor radon activity concentration in two villages of West-Khasi hills district of Meghalaya, India. *AIP Conf. Proc.* **1951**, 020011 (2018).
11. Pyngrope, A. et al. Study of indoor radon, thoron and their progeny in South West Khasi Hills district of Meghalaya, India. *Radiat. Prot. Dosimetry* **189**, 347–353 (2020).
12. Pyngrope, A. & Saxena, A. Radiation exposure due to indoor radon and thoron in the environs of Jowai Town, Meghalaya, India. In *Selected Progresses in Modern Physics* (eds. Sengupta, S. et al.). 277–284 (Springer Singapore, 2021).
13. Ryngna, J. T., Jyrwa, B. M., Nandy, M. & Saxena, A. Natural radioactivity and assessment of hazard indices of the soil found at Sung Valley, Meghalaya. *Radiat. Prot. Dosimetry* **199**, 623–630 (2023).
14. Pyngrope, A., Saxena, A., Khardewasaw, A., Sharma, Y. & Sahoo, B. K. Effect of soil's porosity and moisture content on radon and thoron exhalation rates. *J. Radioanal. Nucl. Chem.* **331**, 1975–1984 (2022).
15. Lyngdoh, A. T. G. & Purkayastha, S. Rainfall trend analysis of the Northern slopes of the Meghalaya Plateau: A case study of Ri Bhoi district. *Int. J. Ecol. Environ. Sci.* **50**, 405–411 (2024).
16. Isinkaye, M. O. et al. Radiotoxicity and health risk assessment of 222Rn in groundwater using statistical and Monte Carlo simulation approaches. *Groundw. Sustain. Dev.* **21**, 100924 (2023).
17. Pyuskyulyan, K. et al. Assessing radon hazard in drinking water: A comprehensive approach integrating deterministic and probabilistic methods with water consumption routines. *Sci. Total Environ.* **949**, 175217 (2024).
18. Akhil, R. V., Joseph, S. & Sukanya, S. Health risk assessment of radon in groundwater of a tropical river basin, SW India. *J. Radioanal. Nucl. Chem.* **333**, 1707–1718 (2024).

19. IAEA. Guidelines on soil and vegetation sampling for radiological monitoring. *Int. At. Energy Agency* 1–247 (2019). <https://www.iaea.org/publications/12219/guidelines-on-soil-and-vegetation-sampling-for-radiological-monitoring>
20. ASTM. *Standard Test Method for Radon in Drinking Water*. <https://www.astm.org/d5072-09r16.html> (2016). <https://doi.org/10.1520/D5072-09R16>
21. Rangaswamy, D. R., Srinivasa, E., Srilatha, M. C. & Sannappa, J. Measurement of radon concentration in drinking water of Shimoga district, Karnataka, India. *J. Radioanal Nucl. Chem.* **307**, 907–916 (2016).
22. Eappen, K. P., Nair, R. N. & Mayya, Y. S. Simultaneous measurement of radon and thoron using Lucas scintillation cell. *Radiat. Meas.* **43**, 91–97 (2008).
23. Sannappa, J., Suresh, S., Rangaswamy, D. R. & Srinivasa, E. Estimation of ambient gamma radiation dose and drinking water radon concentration in coastal taluks of Uttara Kannada district, Karnataka. *J. Radioanal Nucl. Chem.* **323**, 1459–1466 (2020).
24. USEPA. *Proposed Radon in Drinking Water Rule Technical Fact Sheet*. 1–6 (1999). <https://nepis.epa.gov/Exe/ZyPURL.cgi?Dockey=PL008HLV.txt>
25. WHO. *Guidelines for Drinking-Water Quality; Fourth Edition Incorporating the First and Second Addendum* (World Health Organization, 2022).
26. UNSCEAR. *Sources and Effects of Ionizing Radiation, United Nations Scientific Committee on the Effects of Atomic Radiation (UNSCEAR) 2000 Report, Volume I: Report To the General Assembly, with Scientific Annexes-Sources* (United Nations (UN), 2000). <https://doi.org/10.18356/49c437f9-en>
27. Paquet, F. et al. ICRP publication 137: occupational intakes of radionuclides: part 3. *Ann. ICRP.* **46**, 1–486 (2017).
28. Kumar, M., Sahoo, B., Kumar, R. & Sharma, N. Estimation of radon exhalation rate from a brick wall during various stages of construction by measuring exhalation rates from various building materials. *Radiation Prot. Environ.* **43**, 31 (2020).
29. Duggal, V., Sharma, S. & Mehra, R. Risk assessment of radon in drinking water in khetri copper belt of Rajasthan, India. *Chemosphere* **239**, 124782 (2020).
30. ICRP. *Summary of ICRP Recommendations on Radon*. (2018). <http://www.icrpaedia.org/images/f/fd/ICRPRadonSummary.pdf>
31. UNSCEAR. *Sources and Effects of Ionizing Radiation: United Nations Committee on the Effects of Atomic Radiation : UNSCEAR 1993 Report to the General Assembly, with Scientific Annexes* (United Nations, 1993).
32. Lecomte, J. F. et al. ICRP publication 126: radiological protection against radon exposure. *Ann. ICRP.* **43**, 5–73 (2014).
33. Kayakökü, H. & Kuluöztürk, M. F. Radon risk assessment and dose rates in Hekimhan and Kuluncak (Malatya, Turkey) soil samples. *Water Air Soil. Pollut.* **234**, 95 (2023).
34. Szewczak, K. et al. Radon emission fluctuation as a result of biochar application into the soil. *Sci. Rep.* **11**, 13810 (2021).
35. Jaishi, H. P., Singh, S., Tiwari, R. P. & Tiwari, R. C. Analysis of subsurface soil radon with the environmental parameters and its relation with seismic events. *J. Geol. Soc. India.* **99**, 847–858 (2023).
36. Tiwari, R. C., Jaishi, H. P., Singh, S. & Tiwari, R. P. A study of soil radon and seismicity along active fault region in Northeastern India. *Arab. J. Geosci.* **16**, 253 (2023).
37. Eappen, K. P. & Mayya, Y. S. Calibration factors for LR-115 (type-II) based radon thoron discriminating dosimeter. *Radiat. Meas.* **38**, 5–17 (2004).
38. Mahur, A. K., Khan, S., Naqvi, M., Prasad, A. H., Azam, A. & R. & Measurement of effective radium content of sand samples collected from Chhatrapur Beach, Orissa, India using track etch technique. *Radiat. Meas.* **43**, S520–S522 (2008).
39. Shivanandappa, K. C. & Yerol, N. Radon concentration in water, soil and sediment of Hemavathi River environments. *Indoor Built Environ.* **27**, 587–596 (2017).
40. Thabayneh, K. M. Determination of radon exhalation rates in soil samples using sealed can technique and CR-39 detectors. *J. Environ. Health Sci. Eng.* **16**, 121–128 (2018).
41. Stoulos, S., Manolopoulou, M. & Papastefanou, C. Assessment of natural radiation exposure and radon exhalation from building materials in Greece. *J. Environ. Radioact.* **69**, 225–240 (2003).
42. Righi, S. & Bruzzi, L. Natural radioactivity and radon exhalation in building materials used in Italian dwellings. *J. Environ. Radioact.* **88**, 158–170 (2006).
43. Bruzzi, L., Mele, R. & Padoani, F. Evaluation of gamma and alpha doses due to natural radioactivity of building materials. *J. Radiol. Prot.* **12**, 67 (1992).
44. Devi, V., Kumar, A. & Chauhan, R. P. A study on radionuclides content and radon exhalation from soil of Northern India. *Environ. Earth Sci.* **78**, 1–12 (2019).
45. Hassan, N. et al. Assessment of the natural radioactivity using two techniques for the measurement of radionuclide concentration in building materials used in Japan. *J. Radioanal Nucl. Chem.* **283**, 15–21 (2009).
46. Borgohain, D., Lanong, S. & P Jaishi, H. Heavy metal contamination and health risks in ground water at Byrnihat industrial area: urgent need for remediation and public health safeguards. *Proc. Indian Natl. Sci. Acad.* **90**, 931–942 (2024).
47. Cohen, J. Statistical power analysis for the behavioral sciences. *Stat. Power Anal. Behav. Sci.* <https://doi.org/10.4324/9780203771587> (2013).
48. Sahu, P., Panigrahi, D. C. & Mishra, D. P. Sources of radon and its measurement techniques in underground uranium mines – An overview. *J. Sustainable Min.* **13**, 11–18 (2014).
49. Sadiq, M., Umrao, R. K. & Dutta, J. C. Occurrence of rare Earth elements in parts of Nongpoh granite, Ri-Bhoi district, Meghalaya. *Curr. Sci.* **106**, 162–165 (2014).
50. Sadiq, M. et al. Mineralogy, geochemistry and geochronology of mafic magmatic enclaves and their significance in evolution of Nongpoh granitoids, Meghalaya, NE India. *Geol. Soc. Spec. Publ.* **463**, 171–198 (2018).
51. CGWB. Government of India Ministry of Water Resources Technical Report. Series: D. (2013). https://www.cgwb.gov.in/old_web/site/District_Profile/Meghalaya/Ri%20Bhoi.pdf
52. Zhang, S., Shi, Z., Wang, G., Yan, R. & Zhang, Z. Groundwater radon precursor anomalies identification by decision tree method. *Appl. Geochem.* **121**, 104696 (2020).
53. Nam, Y. et al. Radon concentration and affecting environmental conditions in water-curtain heated cultivation facilities. *Helyon* **10** (2024).
54. Haquin, G., Zafirir, H., Ilzycer, D. & Weisbrod, N. Effect of atmospheric temperature on underground radon: A laboratory experiment. *J. Environ. Radioact.* **253–254**, 106992 (2022).
55. Sukanya, S., Noble, J. & Joseph, S. Factors controlling the distribution of radon (222Rn) in groundwater of a tropical mountainous river basin in Southwest India. *Chemosphere* **263**, 128096 (2021).
56. Cho, J. S., Ahn, J. K., Kim, H. C. & Lee, D. W. Radon concentrations in groundwater in Busan measured with a liquid scintillation counter method. *J. Environ. Radioact.* **75**, 105–112 (2004).
57. Deepika, D. N. et al. Radiological assessment of radium and dissolved radon in groundwater near the Manchanabele Reservoir, Bengaluru, India. *Radiat. Phys. Chem.* **233**, 112735 (2025).
58. Pandith, T. A. et al. Exploring tectonic sites with radon from groundwater sources and dose evaluation in various age groups in Baramulla, J&K, India. *Groundw. Sustain. Dev.* **26**, 101232 (2024).
59. Xinwei, L. Analysis of radon concentration in drinking water in Baoji (China) and the associated health effects. *Radiat. Prot. Dosimetry* **121**, 452–455 (2006).
60. Prasad, N. G. S., Nagaiah, N., Ashok, G. V. & Mahesh, H. M. Radiation dose from dissolved radon in potable waters of the Bangalore environment, South India. *Int. J. Environ. Stud.* **64**, 83–92 (2007).

61. Galán López, M. Martín Sánchez, A. Present status of 222Rn in groundwater in Extremadura. *J. Environ. Radioact.* **99**, 1539–1543 (2008).
62. Abdurabu, W. A., Ramli, A. T., Saleh, M. A. & Heryansyah, A. The activity concentrations of 222Rn and corresponding health risk in groundwater samples from basement and sandstone aquifer; the correlation to physicochemical parameters. *Radiat. Phys. Chem.* **127**, 34–41 (2016).
63. Hassan, R. A., Aldaihani, N., Almatani, T. U. & Matar, H. Evaluation of the groundwater radon concentration in the al Jahra Governorate, Kuwait. *J. Radiat. Res. Appl. Sci.* **17**, 100903 (2024).
64. Mukherjee, J., Mitra, S., Sutradhar, S., Mondal, S. & Barman, C. Radon (Rn-222) activity measurement in ground water and associated dose estimation in Raghunathpur and Jhalda municipalities of purulia district, West Bengal, India. *J. Radioanal. Nucl. Chem.* **333**, 1427–1441 (2024).
65. Tairi, A., Bouchaou, L., Hssaisoune, M., Bentahar, Z. & Mostafa, M. Y. A. Exploring radon risk in groundwater: insights from few investigated areas in Morocco. *Environ. Earth Sci.* **83**, 396 (2024).
66. Said, K. et al. Assessing carcinogenic radon levels in water from Er-Rachidia, Morocco using LR-115 nuclear track detectors. *Radiochim. Acta.* **113**, 255–261 (2024).
67. Shah, S. S. A. et al. Geographical distribution of radon and associated health risks in drinking water samples collected from the Mulazai area of Peshawar, Pakistan. *Sci. Rep.* **14**, 6042 (2024).
68. Jamir, S., Sahoo, B. K., Mishra, R. & Sinha, D. Estimation of radon in groundwater and analysis of radon and thoron exhalation rates of the soil in Mokokchung district, Nagaland, India. *Groundw. Sustain. Dev.* **20**, 100874 (2023).
69. Mamun, A. & Alazmi, A. S. Risk assessment of radon exposure by ingestion and inhalation of groundwater within different age groups. *Groundw. Monit. Remediation.* **43**, 69–77 (2023).
70. Shu'aibu, H. K., Khandaker, M. U., Baballe, A., Tata, S. & Adamu, M. A. Determination of radon concentration in groundwater of Gadau, Bauchi State, Nigeria and estimation of effective dose. *Radiat. Phys. Chem.* **178**, 108934 (2021).
71. El-Araby, E. H., Soliman, H. A. & Abo-Elmagd, M. Measurement of radon levels in water and the associated health hazards in Jazan, Saudi Arabia. *J. Radiat. Res. Appl. Sci.* **12**, 31–36 (2019).
72. USEPA. *Exposure Factors Handbook*. (United States Environmental Protection Agency, 2011). <https://www.epa.gov/expobox/exposure-factors-handbook-2011-edition> (2011).
73. Lara, E. et al. Radon concentration in soil gas and its correlations with pedologies, permeabilities and 226Ra content in the soil of the metropolitan region of Belo Horizonte – RMBH, Brazil. *Radiat. Phys. Chem.* **116**, 317–320 (2015).
74. Singh, B. & Kant, K. Estimation of exhalation rates of radon and thoron in the soil samples collected from Gurugram, Haryana, India. *Indian J. Pure Appl. Phys. (IJPAP).* **61**, 938–944 (2023).
75. Nath, K. et al. Neotectonism and reactivation of tectonic elements in Eastern part of Shillong Plateau, India: Constraints from morpho-tectonic analyses. *Geol. Ecol. Landscapes.* <https://doi.org/10.1080/24749508.2024.2338973>;PAGE:STRING:ARTICLE/CHAPTER.
76. Gogoi, P. P., Phukan, S. & Barooah, D. Measurements of 222Rn exhalation rates, effective 226Ra contents, and radiological risks from geological samples of Kopili fault zone and gneissic complex of Shillong Plateau, India. *Radiochim. Acta.* **112**, 183–195 (2024).
77. Adelbert Kharlyngdoh, C. Z. P. K. B. P. T. D. B. U. C. A. K. S. Characterization and classification of soils in Eastern Himalayan Agro-climatic region: A case study in Nongpoh Micro-watershed of Ri-Bhoi District, Meghalaya. *J. Indian Soc. Soil. Sci.* **63** (2015).
78. Celen, Y. Y., Gunay, O., Oncul, S. & Narin, B. Measurement of soil radon concentration in Balikesir and examination of its effects on health. *J. Radiat. Res. Appl. Sci.* **16**, 100718 (2023).
79. Hanfi, M. Y. et al. Radiation doses assessment and radon exhalation rate from the soils of Albyda area, Yemen. *Nuclear Eng. Technol.* **57**, 103227 (2025).
80. ICRP. *Protection Against Radon-222 at Home and at Work*. ICRP Publication 65. Ann. ICRP. Vol. 23. (Pergamon, 1993).
81. CDC. Radiation and your health: Facts about radiation from building materials. (U S Centers Disease Control Prevention, 2024). <https://www.cdc.gov/radiation-health/data-research/facts-stats/building-materials.html>
82. USEPA. US EPA. Natural radioactivity in building materials. (United States Environmental Protection Agency, 2025). <https://www.epa.gov/raddown/natural-radioactivity-building-materials>
83. Pyngrope, A., Kakati, R. K. & Dkhar, P. Study of radon and thoron exhalation rates in common building materials of Jowai region Meghalaya, India. *J. Radioanal. Nucl. Chem.* <https://doi.org/10.1007/s10967-024-09949-x> (2024).
84. WHO. *WHO Handbook on Indoor Radon: A Public Health Perspective* (World Health Organization, 2009).
85. Benà, E. et al. A new perspective in radon risk assessment: mapping the geological hazard as a first step to define the collective radon risk exposure. *Sci. Total Environ.* **912**, 169569 (2024).
86. Baskaran, M. Radon measurement techniques. In: Radon: A Tracer for Geological, Geophysical and Geochemical Studies. 15–35. https://doi.org/10.1007/978-3-319-21329-3_2. (Springer, 2016).
87. Dwaikat, N., Safarini, G., El-hasan, M. & Iida, T. CR-39 detector compared with Kodalpha film type (LR115) in terms of radon concentration. *Nucl. Instrum. Methods Phys. Res. A.* **574**, 289–291 (2007).
88. Guo, S. L., Chen, B. L. & Durrani, S. A. Solid-State Nuclear Track Detectors. in *Handbook of Radioactivity Analysis*. 233–298 (Academic Press, 2012). <https://doi.org/10.1016/B978-0-12-384873-4.00004-9>

Acknowledgements

The authors would like to thank the University of Science and Technology Meghalaya (USTM) for providing the instruments to carry out this research.

Author contributions

All authors contributed to the study conception and design. H.P.J. performed Formal analysis, original draft preparation, writing, review, editing & overall supervision. D.B. performed the Investigation and experimental analysis. R.C.T. contributed to experimental procedure, review, editing and supervision. S.K. performed the data collection and experimental analysis. S.R. performed the data collection and experimental analysis. A.Z. performed the data collection and experimental analysis. All authors read and approved the final manuscript.

Declarations

Competing interests

The authors declare no competing interests.

Additional information

Correspondence and requests for materials should be addressed to H.P.J.

Reprints and permissions information is available at www.nature.com/reprints.

Publisher's note Springer Nature remains neutral with regard to jurisdictional claims in published maps and institutional affiliations.

Open Access This article is licensed under a Creative Commons Attribution-NonCommercial-NoDerivatives 4.0 International License, which permits any non-commercial use, sharing, distribution and reproduction in any medium or format, as long as you give appropriate credit to the original author(s) and the source, provide a link to the Creative Commons licence, and indicate if you modified the licensed material. You do not have permission under this licence to share adapted material derived from this article or parts of it. The images or other third party material in this article are included in the article's Creative Commons licence, unless indicated otherwise in a credit line to the material. If material is not included in the article's Creative Commons licence and your intended use is not permitted by statutory regulation or exceeds the permitted use, you will need to obtain permission directly from the copyright holder. To view a copy of this licence, visit <http://creativecommons.org/licenses/by-nc-nd/4.0/>.

© The Author(s) 2025